



Article

Structural Evolution of Polyimide-Derived Carbon during Phosphoric Acid Activation

Alexander M. Puziy ^{1,*}, Olga I. Poddubnaya ¹, Barbara Gawdzik ², Magdalena Sobiesiak ² and Myroslav Sprynskyy ³

¹ Department of Chemistry and Chemical Technology, National Aviation University, 1 Liubomyr Huzar Prospect, 03058 Kyiv, Ukraine

² Department of Polymer Chemistry, Maria Curie-Skłodowska University, ul. Gliniana 33, 20-614 Lublin, Poland

³ Department of Environmental Chemistry and Bioanalytics, Faculty of Chemistry, Nicolaus Copernicus University in Torun, 7 Gagarina Str, 87-100 Torun, Poland

* Correspondence: alexander.puziy@gmail.com

Abstract: Carbon adsorbents were obtained by carbonization of polyimide polymer with and without the presence of phosphoric acid at temperatures in the range of 400–1000 °C. Carbons produced in the presence of phosphoric acid have been demonstrated to contain up to 13.2% phosphorus. The structure of phosphorus-containing compounds was investigated by XPS and ³¹P MAS NMR methods. Deconvolution of the P 2p peak with variable binding energy showed the presence of only phosphates/polyphosphates. However, a low value of the O/P ratio is an indirect indication of the possible presence of phosphonates. A ³¹P MAS NMR study revealed the existence of several kinds of phosphates as well as a minor quantity (1–9%) of phosphonates. All discovered phosphorus-containing compounds are acidic and therefore give carbon the ability to absorb metal cations. The study of copper ion adsorption demonstrated that phosphorus-containing carbon shows a significant adsorption capability even in extremely acidic conditions. At pH 3–6, phosphorus-containing carbon may completely remove copper from the aqueous solution. Phosphorus-containing carbon has a higher adsorption capacity for copper ions than ion exchange resins with carboxyl or sulfo groups.

Keywords: phosphorus-containing carbon; XPS; ³¹P MAS NMR; surface groups; acid-base properties; metal ion binding



Citation: Puziy, A.M.; Poddubnaya, O.I.; Gawdzik, B.; Sobiesiak, M.; Sprynskyy, M. Structural Evolution of Polyimide-Derived Carbon during Phosphoric Acid Activation. *C* **2022**, *8*, 47. <https://doi.org/10.3390/c8030047>

Academic Editors: Sergey Mikhalovsky and Rosa Busquets

Received: 18 August 2022

Accepted: 14 September 2022

Published: 19 September 2022

Publisher's Note: MDPI stays neutral with regard to jurisdictional claims in published maps and institutional affiliations.



Copyright: © 2022 by the authors. Licensee MDPI, Basel, Switzerland. This article is an open access article distributed under the terms and conditions of the Creative Commons Attribution (CC BY) license (<https://creativecommons.org/licenses/by/4.0/>).

1. Introduction

The activation of various precursors with phosphoric acid is a widely used industrial process for the production of highly porous carbon adsorbents [1–7]. Phosphoric acid activation has several advantages, primarily high yields and low activation temperatures compared to physical activation [8–10]. In addition, phosphoric acid activation does not have the disadvantages, such as corrosion problems, insufficient recovery of the activator, and environmental problems inherent in the zinc chloride activation process [11].

Many scientists, however, are unaware of the possible inclusion of phosphorous compounds into the carbon structure during activation with phosphoric acid, which can modify the surface chemistry of the carbon adsorbent. Recently it was shown that phosphorus compounds, which are incorporated into the structure during activation with phosphoric acid, give an acidic character to the surface of activated carbon, which determines their catalytic properties and adsorption capacity for metal ions [12]. The XPS technique is most commonly used to identify the structure of phosphorus compounds in phosphorus-containing carbon materials [13–17]. However, there are disagreements in the literature regarding the interpretation of experimental XPS spectra, which may lead to different conclusions regarding the structure of phosphorus-containing compounds. On the one hand, some researchers conduct deconvolution of the P 2p peak with varying binding

energy and assign the resulting values to specific substances with close binding energy. New peaks are added until there is no increase in the quality of fit [15–22]. On the other hand, other investigators perform deconvolution of the P 2p region to 3–4 peaks with *a priori* fixed binding energy values corresponding to certain phosphorus compounds [23–28]. Thus, different structures of phosphorus-containing compounds in activated carbon can be obtained from the same P 2p spectrum depending on the deconvolution scheme. The use of an auxiliary method, such as ^{31}P NMR, can assist in identifying the structure of phosphorus compounds in carbon adsorbents and predicting their characteristics [22,29–37].

In this study, an analysis of the structure of phosphorus-containing compounds in activated carbons obtained from polyimides was carried out using XPS and NMR techniques and the relationship of the structure with acid-base characteristics and adsorption capacity for copper ions is established.

2. Materials and Methods

2.1. Precursor Polymer

Porous polyimide copolymer, designated as BM-DVB, was chosen as the raw material for the production of carbon adsorbents in this study. The initial BM-DVB copolymer was obtained by suspension polymerization of 4,4'-bis(maleimidodiphenyl) methane (50 mol percent) and divinylbenzene (50 mol percent) in the presence of a pore former (a mixture of decyl alcohol and benzyl alcohol) [38]. The chemical structure of BM-DVB is shown in Figure 1.

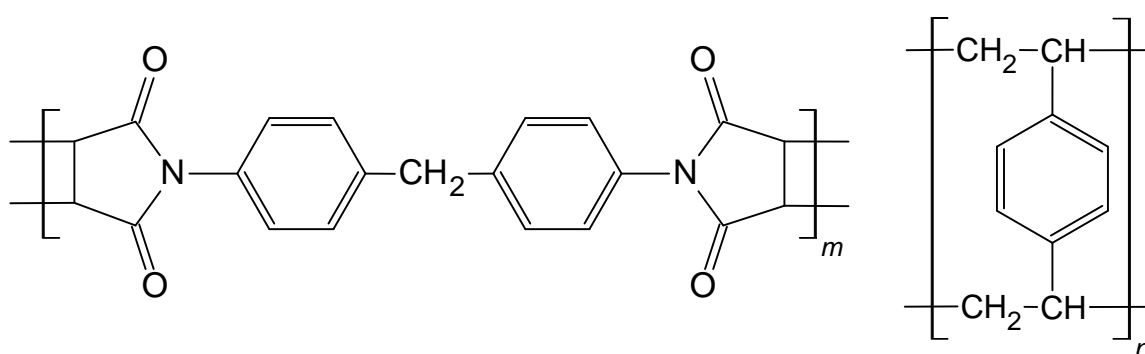


Figure 1. The chemical formula of 4,4'-bis(maleimidodiphenyl) methane.

2.2. Synthesis of Carbon Adsorbents

Carbon adsorbents were obtained by carbonization of BM-DVB porous copolymer impregnated with phosphoric acid (acid/precursor ratio 1:1) at temperatures 400–1000 °C in argon flow (H_3PO_4 series) [39–43]. After carbonization, carbons were thoroughly washed with hot water in the Soxhlet extractor until the wash waters reached neutral pH. To investigate the involvement of phosphoric acid in the polymer-to-carbon transition, the second series of carbons were produced at the same temperature range without the addition of phosphoric acid (Thermal series).

2.3. Porous Structure

The porous structure of carbons was characterized by nitrogen adsorption measured at -196 °C using the Autosorb-6 adsorption analyzer (Quantachrome, Boynton Beach, FL, USA). Pore size distribution was calculated by SAIEUS software version 2.0 (www.saieus.com) (accessed on 2 March 2015) using a slit pore model incorporating surface energetical heterogeneity and geometrical corrugation [44–46]. The specific surface area, A_{BET} , was calculated by the BET method using nitrogen adsorption data in the relative pressure range chosen using consistency criteria [47]. The total, V_{tot} , micropore, V_{mi} , and mesopore, V_{me} , volumes were calculated from the cumulative pore size distributions as the volume of pores with sizes 50 nm, less than 2 nm, and between 2 and 50 nm, respectively.

2.4. XPS

XPS spectra were obtained using a high vacuum ($<8 \times 10^{-9}$ mbar) multi-chamber UHV system (Prevac, Poland) equipped with Al K α line excitation source VG Scienta SAX 100 (12 kV, 30 mA), monochromator VG Scienta XM 780 and hemispherical analyzer Scienta R4000 (VG Scienta AB, Uppsala, Sweden). The pass energy and energy steps were 200 eV and 0.5 eV at the survey spectra and 50 eV and 0.1 eV at the detailed spectra. During the measurement of carbons obtained at 400–600 °C without phosphoric acid, flooding the sample with low-energy electrons was used to neutralize the surface charge. The spectra were calibrated for a carbon C 1s excitation at a binding energy of 284.7 eV.

The spectra were analyzed and processed with the use of CasaXPS software version 2.3.15 (Casa Software LTD., Teignmouth, UK, casaxps.com, accessed on 2 March 2015). After subtraction of the Shirley-type background, curve fitting was performed using a mixed 30% Gaussian–Lorentzian peak shape. The P 2p curves were fitted taking into account the spin-orbit splitting of 0.85 eV [48,49] and the intensity ratio of the 2p_{1/2}:2p_{3/2} components as 1:2. The composition (in at%) was determined by considering the integrated peak areas of C 1s, N 1s, O 1s and P 2p from the survey spectra and the respective sensitivity factors [50].

2.5. ³¹P MAS NMR

Nuclear magnetic resonance (NMR) spectra were acquired in the solid state with magic angle spinning (MAS) using a Bruker Avance III HD 400WB spectrometer (Bruker, Billerica, MA, USA) at room temperature. ³¹P MAS NMR spectra were recorded in a single-pulse sequence with a pulse width of 2 ms, a relaxation time of 5 s, and a spinning frequency of 18 kHz. An 85% H₃PO₄ aqueous solution was used as an external reference for the ³¹P MAS NMR chemical shift.

2.6. Acid-Base Properties

Acid-base properties of polyimide-derived carbons were investigated by potentiometric titration [51] performed in a thermostatic vessel at 25 °C using a 672 Titroprocessor combined with 655 Dosimat (Metrohm, Herisau, Switzerland). To prevent contamination with CO₂, the flow of pure argon was used throughout the titration. The proton concentration was monitored using an LL pH glass electrode (Metrohm, Herisau, Switzerland). Before experiments, the electrode electromotive force was calibrated to proton concentration by blank titration. Solution equilibria and a correction for possible carbonate and silicate contaminations were calculated using EST software [52]. Proton affinity distributions, F(pK_a), were calculated from proton-binding isotherms by solving the adsorption integral equation using the CONTIN method [53–56].

2.7. Copper Binding

The batch technique was used for the determination of copper adsorption. Weighed amounts of adsorbent (0.1 ± 0.0001 g) were placed into Erlenmeyer flasks. A volume of 20 mL containing 0.1 M NaCl solution as background electrolyte and 0.001 M copper ion solution was added to each flask. Then different amounts of either 0.1 M HCl or 0.1 M NaOH were added to change the solution pH. To attain equilibrium the flasks were shaken for 24 h. After equilibration, the pH was measured with a glass electrode and the metal ion concentration was determined titrimetrically with EDTA. Copper binding is given in dimensionless units, defined as the quantity of adsorbed copper divided by the total amount of copper in the adsorption system.

3. Results and Discussion

3.1. Porous Structure

Nitrogen adsorption-desorption isotherm for parent BM-DVB copolymer belongs to type II of IUPAC classification [57] characteristic to adsorption on nonporous or macroporous adsorbents (Figure 2a). On the contrary, the isotherms for carbons obtained by

carbonization of BM-DVB copolymer can be attributed to a combination of type I and IVa of IUPAC classification. A steep rise of nitrogen uptake at very low p/p^0 is due to adsorption in narrow micropores with enhanced potential while the gradual increase in nitrogen adsorption at medium to high relative pressures corresponds to monolayer-multilayer adsorption in mesopores followed by capillary condensation accompanied by small hysteresis of type H4. The isotherms are typical of micro-mesoporous carbons.

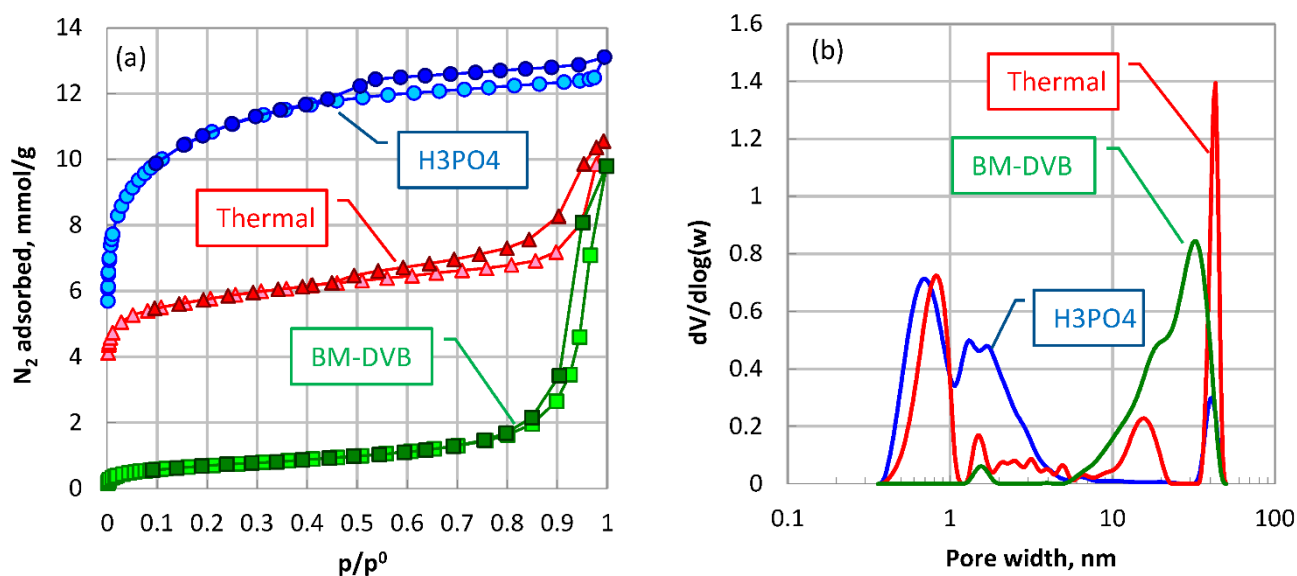


Figure 2. Nitrogen adsorption-desorption isotherms: (a) and pore size distributions; and (b) for parent BM-DVB copolymer and carbons obtained by carbonization at 600 °C of polyimide copolymer in the presence of phosphoric acid (H₃PO₄) and without acid (Thermal).

The pore size distribution in the porous polymer BM-DVB reveals a developed mesoporous structure in the range of pores from 12 to 44 nm, with a maximum at 34 nm and the absence of micropores (Figure 2b). Carbonization of a porous polymer in the presence of phosphoric acid results in a complete restructuring of the porous structure, with well-developed porosity appearing in the range of micropores and small mesopores (0.5–5 nm) and the polymer's developed mesoporous structure transforming into small rudimentary residues. Carbonization of a porous polymer without phosphoric acid, on the other hand, produces an increase in the size of mesopores and the emergence of a microporous structure. It should be noted that the microporous structure of carbon obtained without phosphoric acid is represented by pores in the range of 0.5–1.2 nm, while carbon obtained in the presence of phosphoric acid has additional pores in the range of 1.2–5 nm.

Carbons produced in the presence of phosphoric acid have a more developed porous structure than carbons formed in the absence of acid (Table 1). Phosphoric acid enhances the formation of a microporous structure during carbonation.

3.2. XPS

XPS is a powerful tool for studying the elemental composition and chemical state of phosphorus in carbon materials. An XPS survey scan revealed that both H₃PO₄ and the Thermal series of carbons contain C, O, and N (Table 2). The Thermal series has a greater carbon content at all temperatures due to the higher oxygen and phosphorus content in carbons activated with phosphoric acid (H₃PO₄ series), which decreases the proportion of carbon. Phosphorus is only found in carbons that have been activated with phosphoric acid. The phosphorus content increases to 13.2% when carbonization temperature rises to 800 °C and decreases at higher temperatures. This phenomenon is explained by the acceleration of the formation of phosphorus-carbon compounds when the activation temperature is raised to 800 °C and the breakdown of these compounds at higher temperatures [12]. The

thermodynamic study discovered that phosphorus compound volatilization is favorable at temperatures greater than 750 °C [12,58]. Furthermore, the thermal gravimetric analysis showed that mass loss in the 800–900 °C temperature range is proportional to phosphorus content [12,59].

Table 1. Porous structure parameters for parent porous copolymer BM-DVB and polyimide-derived carbons obtained with (H₃PO₄-series) and without (Thermal-series) phosphoric acid at different temperatures.

Temperature °C	A _{BET} m ² /g	V _{tot} cm ³ /g	V _{mi} cm ³ /g	V _{me} cm ³ /g
BM-DVB				
	55.9	0.338	0.006 (2%)	0.332 (98%)
H ₃ PO ₄ series				
400	11.5	0.026	0.002 (9%)	0.023 (91%)
500	520.2	0.263	0.197 (75%)	0.066 (25%)
600	891.1	0.422	0.324 (77%)	0.098 (23%)
700	676.3	0.336	0.259 (77%)	0.078 (23%)
800	599.4	0.316	0.228 (72%)	0.088 (28%)
900	659.7	0.337	0.255 (76%)	0.082 (24%)
1000	601.9	0.320	0.231 (72%)	0.090 (28%)
Thermal series				
400	36.5	0.228	0.004 (2%)	0.223 (98%)
500	37.5	0.182	0.006 (3%)	0.176 (97%)
600	491.3	0.349	0.174 (50%)	0.175 (50%)
700	522.0	0.328	0.194 (59%)	0.134 (41%)
800	356.5	0.199	0.129 (65%)	0.070 (35%)
900	223.9	0.171	0.080 (47%)	0.090 (53%)
1000	20.3	0.073	0.002 (2%)	0.071 (98%)

Table 2. Chemical composition (in mass%) of polyimide-derived carbons.

Temperature °C	H ₃ PO ₄ Series				Thermal Series		
	C	O	N	P	C	O	N
400	81.2	12.6	2.6	2.2	79.7	15	5.3
500	74.2	15.2	2.3	6.6	84.2	10.4	5.4
600	74.5	12.3	1.6	11.6	91.1	4.3	4.6
700	68.9	15	3.7	12.4	93.2	2.9	3.9
800	66.1	17.1	3.6	13.2	93.3	3.4	3.3
900	68.6	17.3	3.4	10.6	94.4	3	2.6
1000	75.8	14.1	1.7	8.3	92	3.9	2.6

The C 1s peak was deconvoluted into the six components: C-C sp² bonds at 284.7 eV; C-C sp³ at 285.2 eV; C-O at 286.3 eV; C=O at 287.4 eV; O=C-O- at 288.7 eV and shake-up peak that corresponds to π→π* type transitions at 290.5 eV (Figure 3). The content of sp²-hybridized carbon, which belongs to graphite-like fragments of activated carbon, may be obtained by such deconvolution [60–63]. Carbonization in the presence of phosphoric acid results in a significant increase in the content of sp²-hybridized carbon as the temperature

risks from 400 to 500 °C, as seen in Figure 4a. On the contrary, when the BM-DVB copolymer is carbonized without phosphoric acid, the sp^2 -hybridized content increases over a larger temperature range—from 500 to 800 °C. This demonstrates that phosphoric acid facilitates the formation of the polyaromatic structure of carbon at lower temperatures.

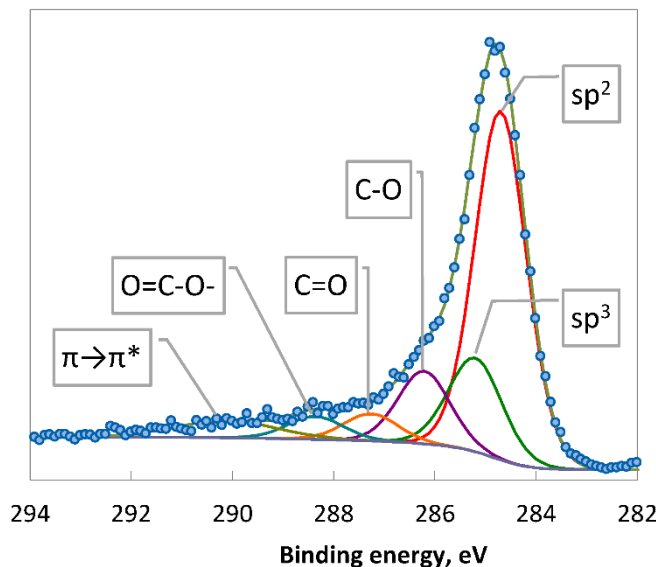


Figure 3. High-resolution X-ray photoelectron spectrum of C 1s peak of polyimide-derived carbon obtained with phosphoric acid at 800 °C.

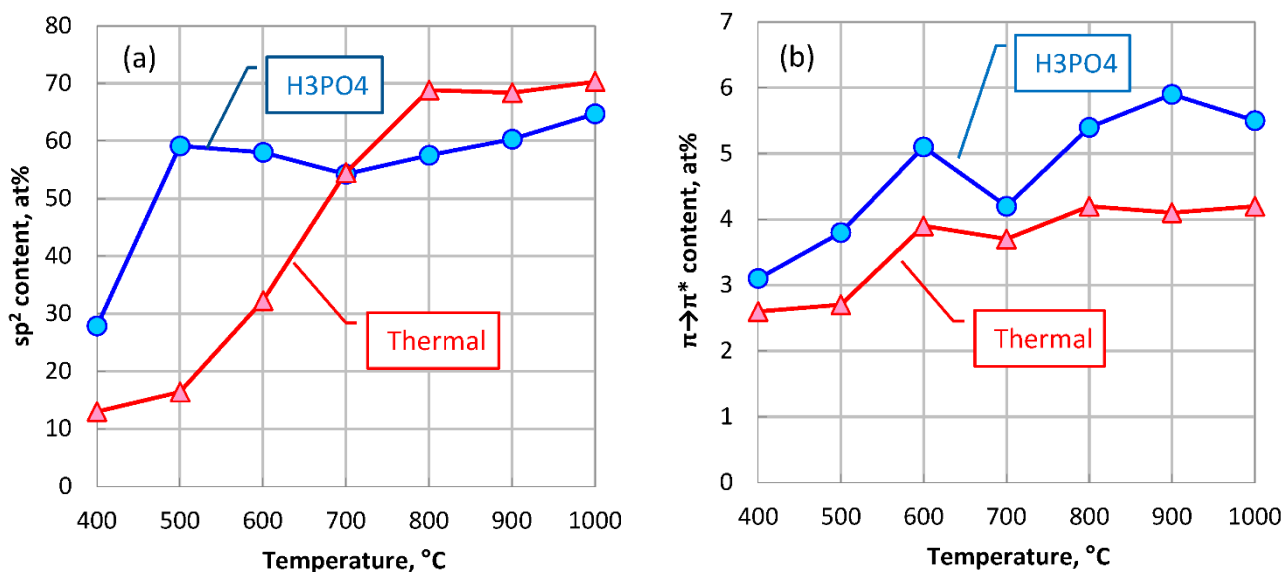


Figure 4. Temperature evolution of sp^2 -hybridized carbon content: (a) and $\pi \rightarrow \pi^*$ shake-up signal (b) of polyimide-derived carbons obtained with (H_3PO_4 -series) and without (Thermal-series) phosphoric acid at different temperatures.

The changes in concentration of π -electrons were also measured by XPS using the $\pi \rightarrow \pi^*$ shake-up signal [64,65]. It is seen that the shake-up signal is consistently higher for phosphoric acid-activated carbons (Figure 4b). However, it should be noted, that the shake-up peaks are superimposed on the broad emission of inelastically scattered electrons, which occurs starting in about the same energy region [64].

Deconvolution of the P 2p envelope revealed only one peak with P 2p 3/2 binding energy of 133.1 ± 0.2 eV (Figure 5a). As the carbonization temperature increases, the binding energy shows some tendency to decrease from 133.4 to 132.8 eV. This peak is relatively

narrow (FWHM 1.9 ± 0.1 eV), confirming the existence of only one type of phosphorus species. Analysis of the NIST X-ray Photoelectron Spectroscopy Database [49] shows that the detected range of binding energies is typical for phosphates and pyrophosphates (Figure 6). A similar classification was made for other phosphorus-containing carbons obtained by phosphoric acid activation of polymer and lignocellulosic materials [15,16,66].

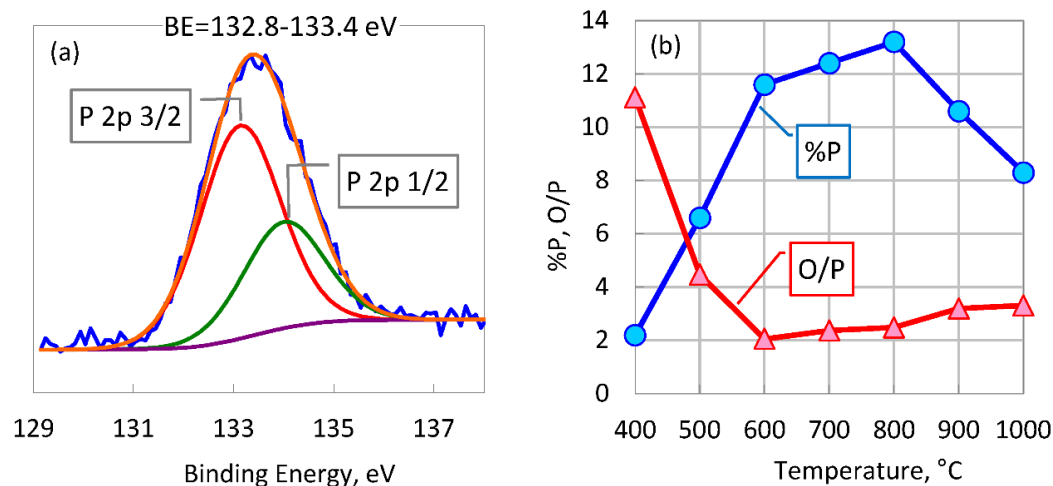


Figure 5. High-resolution X-ray photoelectron spectrum of P 2p peak of polyimide-derived carbon obtained with phosphoric acid at 800 °C (a) and temperature evolution of phosphorus content and atomic O/P ratio (b).

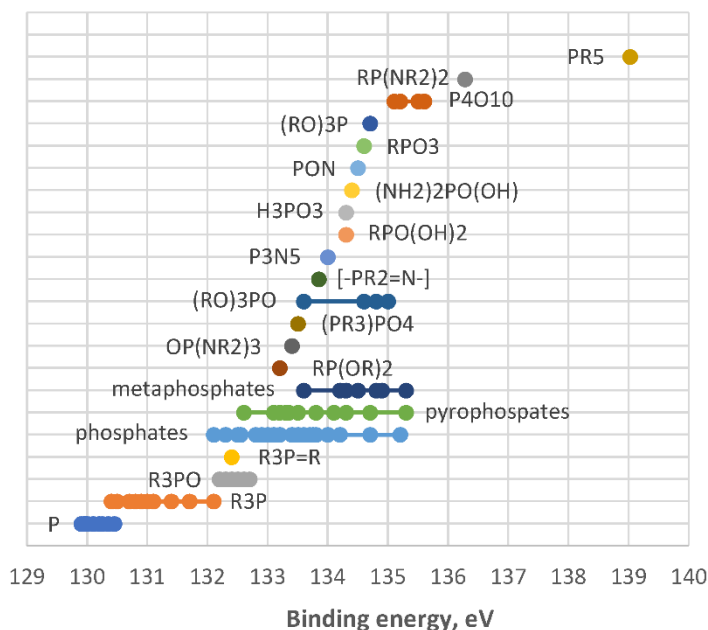


Figure 6. P 2p 3/2 binding energies of different types of phosphorus-containing compounds. Data from NIST X-ray Photoelectron Spectroscopy Database [49].

However, the surface atomic O/P ratio reaches a value of 2.1 for carbon obtained at 600 °C, which suggests the presence of not only phosphates/pyrophosphates (oxyphosphorus compounds with P-O bonds) but also substituted phosphates such as carbophosphorus (P-C bonds) and azaphosphorus (P-N bonds) compounds (Figure 5b).

3.3. ^{31}P MAS NMR

Figure 7a shows ^{31}P MAS NMR spectra of polyimide-derived carbons obtained with phosphoric acid (H_3PO_4 series) at different temperatures. A sharp peak at about 0 ppm and a somewhat broad signal at 7–12 ppm are visible in the ^{31}P NMR spectra. With confidence, phosphate structures may be attributed to the sharp peak. The second signal is rather broad and asymmetric, indicating the presence of a mixture of orthophosphates and/or quadruply attached phosphorus in an asymmetric environment. To reveal these components the spectra were deconvoluted into five peaks using a Lorentzian line shape (Figure 7b). The results of deconvolution are presented in Figure 7b. The peak P1 at around -10 ppm (Figure 8a) only shows up as a shoulder in the main peak P2. The peak P1 may be ascribed to polyphosphate end groups belonging mainly to PO_4 groups linked by one bridging oxygen atom [16,32,35,67–71]. The content of polyphosphates is rather small but increases to 24–26% for carbons obtained at 800–900 °C (Figure 8b). The peak P2 around 0 ppm is sharp and with confidence may be ascribed to orthophosphate structural units linked to polyaromatic graphene framework [16,32,35,67–70]. The peak P2 shifts from 0 to -6.0 ppm with increasing carbonization temperature due to the increasing positive shielding from π -electrons of enlarged graphene layers [16,22,32] (Figure 8a). The peaks P3 and P4 could be ascribed to pyrophosphate diesters [72] and metal phosphates [73]. The formation of pyrophosphate diesters that crosslink the fragments of polymer structure at high temperature is reasonable and was proposed as activating mechanism of phosphoric acid [74]. The highest amount of pyrophosphate diesters is produced around 500 °C, however, when carbonization temperature rises above this point, cross-linking becomes less prominent until it nearly completely disappears at 800–1000 °C (Figure 8b). At high temperatures, orthophosphate structural units become the dominant structure of phosphorus compounds. The peak P5 at 25–30 ppm is ascribed to phosphonates [75]. The content of phosphonates is small at all temperatures and amounts to 1–9%. Thus, the ^{31}P MAS NMR investigation revealed the existence of different types of phosphates as well as phosphonates in the structure of polyimide-derived carbon obtained with phosphoric acid at different temperatures (H_3PO_4 series).

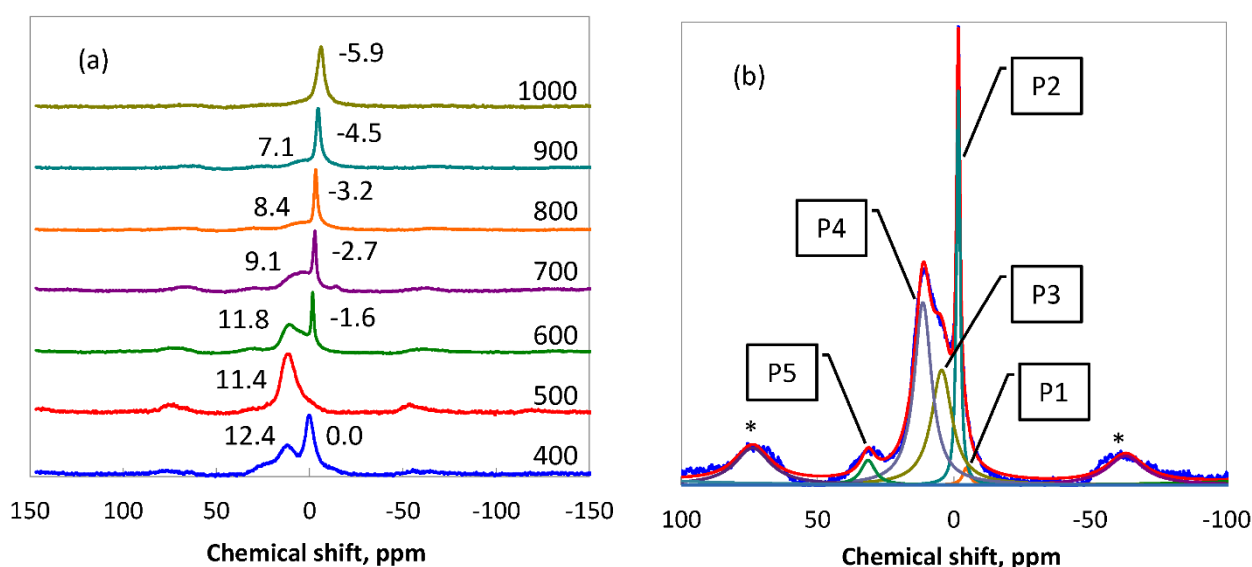


Figure 7. ^{31}P MAS NMR spectra of polyimide-derived carbons obtained with phosphoric acid (H_3PO_4 -series) at different temperatures (a) and deconvolution of ^{31}P MAS NMR spectrum of polyimide-derived carbon obtained with phosphoric acid at 600 °C (b).

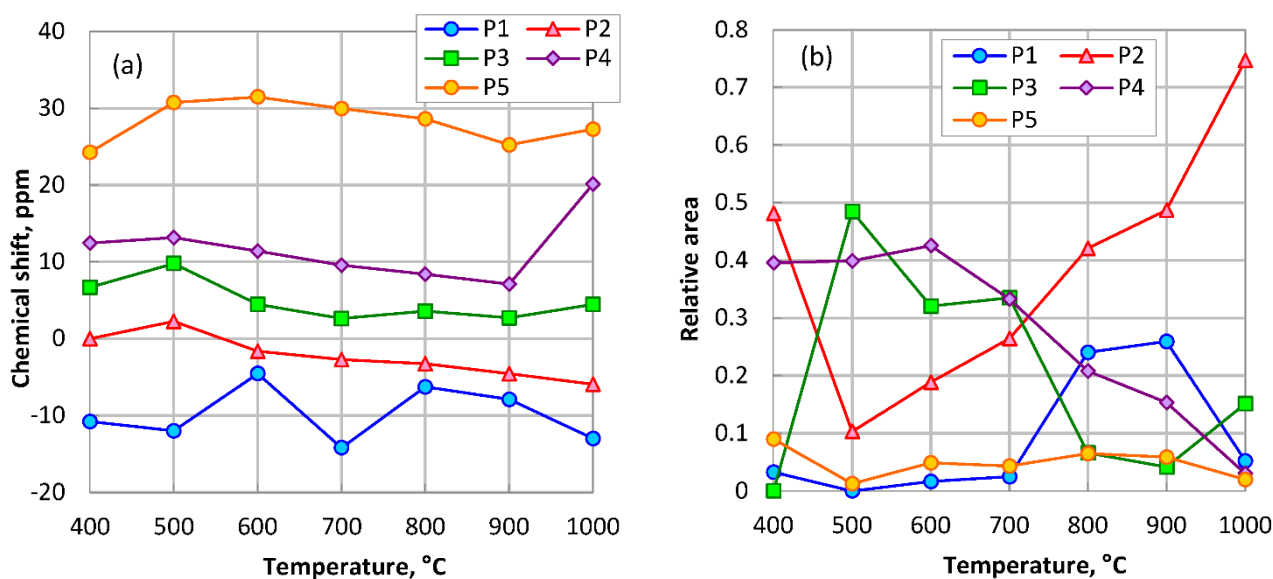


Figure 8. Chemical shift (a) and relative area (b) of deconvoluted components of ^{31}P MAS NMR spectra of polyimide-derived carbons obtained with phosphoric acid (H_3PO_4 -series) at different temperatures.

3.4. Acid-Base Properties

All phosphorus-containing surface compounds discovered by XPS and ^{31}P MAS NMR techniques, including phosphates, pyrophosphates, and phosphonates, are acidic, and their presence in the carbon structure imparts an acidic character. Proton-binding isotherms show that the carbon obtained without phosphoric acid is amphoteric, that is, it is capable of both adsorption of protons in an acidic solution and dissociation of protons in an alkaline medium (Figure 9a). The point of zero charge (PZC), where the sorption of protons is zero, for this carbon is 8.6. On the contrary, the proton-binding isotherm for carbon obtained with phosphoric acid is located entirely in the negative region (Figure 9a). The point of zero charge for this carbon has not even been reached, but extrapolation gives a value of 2.3, which is close to the pK_a of phosphoric acid.

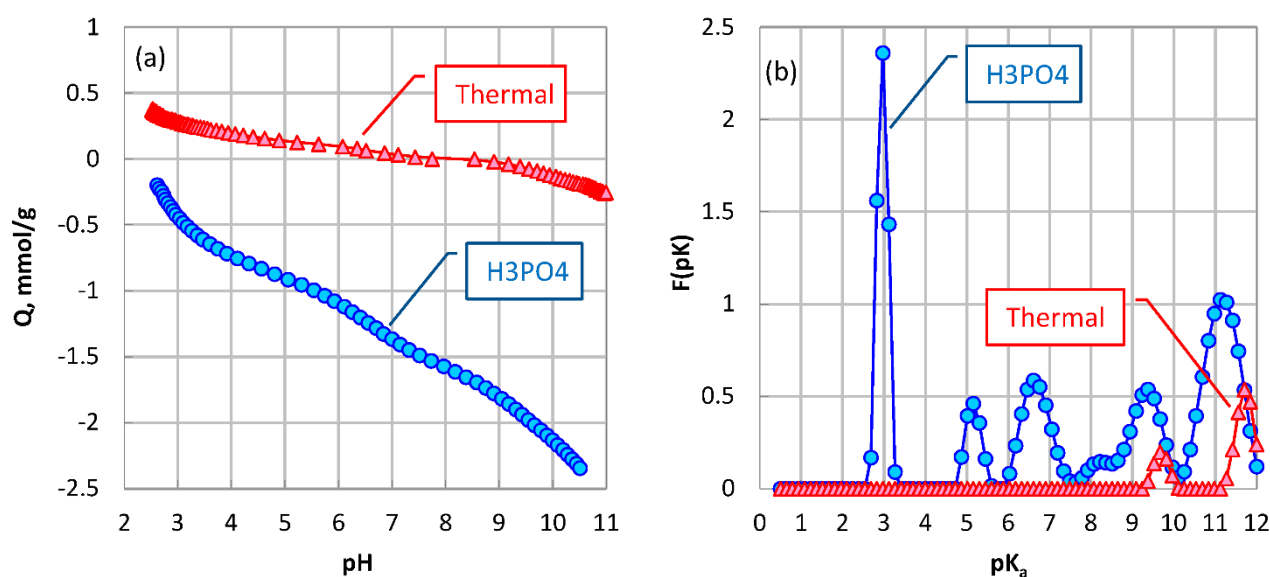


Figure 9. Proton-binding isotherms (a) and proton affinity distributions (b) for polyimide-derived carbons obtained with (H_3PO_4 series) and without (Thermal series) phosphoric acid at 800 °C.

The shape of the proton-binding isotherm for phosphorus-containing carbon is characteristic of multifunctional cation exchangers containing functional groups of different acid strengths. Proton affinity distributions of acid groups calculated by the CONTIN method show two types of acid surface groups for carbon obtained without phosphoric acid (Figure 9b). They can be classed as enol or lactone groups (0.090 mmol/g, pK_a 9.7) and phenolic groups (0.266 mmol/g, pK_a 11.7). Proton affinity distribution for carbon obtained with phosphoric acid shows six types of surface groups that may be classed as phosphates (0.799 mmol/g, pK_{a1} 2.97, 0.515 mmol/g, pK_{a2} 6.69), carboxylic (0.226 mmol/g, pK_a 5.16), and two types of enol and/or lactone (0.107 mmol/g, pK_a 8.21 and 0.494 mmol/g, pK_a 9.33) and phenolic groups (1.118 mmol/g, pK_a 11.16) (Figure 9b). This result shows radically different surface chemistry of carbon obtained with phosphoric acid compared to carbon prepared without acid.

3.5. Copper Binding

Figure 10 shows the pH dependence of copper binding by polyimide-derived carbons obtained with (H_3PO_4 series) and without phosphoric acid (Thermal series). Adsorption of copper ions on all studied adsorbents increases with an increase in the pH of the solution. The increase in copper adsorption with increasing pH occurs due to the deprotonation of surface functional groups and the formation of surface complexes with copper ions [76–80]. Carbon obtained without phosphoric acid shows very small adsorption of copper at $pH < 5.3$ and follows the precipitation curve at higher pHs. This behavior is expected since carbon obtained without phosphoric acid does not have surface groups capable of dissociation at pH less than 5–6.

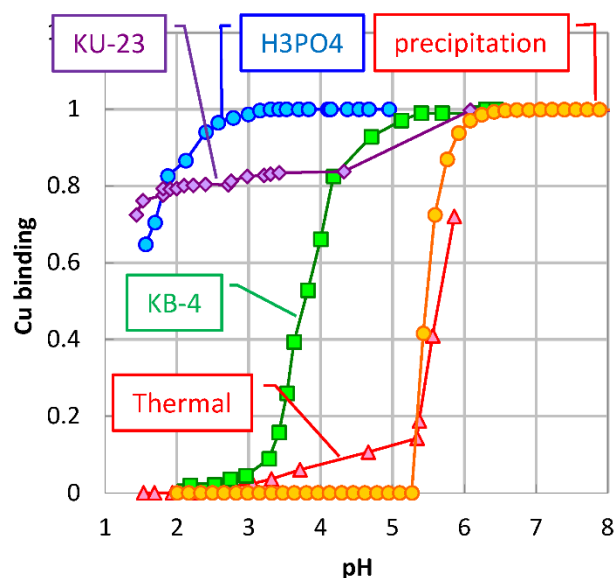


Figure 10. Copper binding by polyimide-derived carbons obtained with (H_3PO_4 -series) and without (Thermal-series) phosphoric acid at 800 °C. Copper binding by ion-exchange resins with carboxyl (KB-4) and sulfo groups (KU-23) is provided for comparison.

On the contrary, the adsorption of copper on polyimide-derived carbon obtained with phosphoric acid is significant even at a very low pH (Figure 10). This carbon exhibits noticeably greater copper adsorption than the cation-exchange resin with carboxylic groups KB-4 (an analog of Amberlite IRC 86), which has a very high cation exchange capacity of 10 mmol/g. Adsorption of copper on the carbon is even greater than that on the very acidic cation exchange resin KU-23 containing sulfo groups (analog to Amberlyst-15) with a cation exchange capacity of 4.5 mmol/g. Despite having a lower cation-exchange capacity of 2.5 mmol/g, phosphorus-containing carbon removes more copper than ion-exchange

resins. This shows that phosphorus-containing carbon has a higher affinity for copper ions than ion-exchange resins.

It is worth noting that polyimide-derived carbon obtained with phosphoric acid exhibits significant copper uptake at pH values lower than PZC (pH < 2.3), i.e., when the surface of carbon is positively charged, and therefore cation adsorption should be hindered. This phenomenon has been reported previously for the adsorption of Cd(II), Hg(II), and Cr(III) and has been explained as being due to an ion exchange reaction between the delocalized protonated π -electrons of the graphene layer of carbon ($-C\pi-H_3O^+$) and the metal cation [81–85]. The high adsorption capacity of polyimide-derived carbon obtained with phosphoric acid in an acidic environment indicates its potential for the extraction of heavy metal ions from acidic solutions, as well as its use as an enterosorbent for detoxification of the body from toxic metals in the acidic environment of the stomach.

4. Conclusions

Carbonization of porous polyimide copolymer results in the formation of carbon adsorbents with a developed porous structure (A_{BET} is up to 891 m²/g). Carbons produced in the presence of phosphoric acid have a more developed porous structure than carbons formed in the absence of acid. Phosphoric acid enhances the formation of a microporous structure during carbonation.

The chemical structure of polyimide-derived carbons obtained with and without phosphoric acid has been investigated by XPS and ³¹P MAS NMR methods. Deconvolution of the P 2p peak with variable binding energy showed the presence of only phosphates/polyphosphates. However, a low value of the O/P ratio is an indirect indication of the possible presence of phosphonates. ³¹P MAS NMR study revealed the existence of several kinds of phosphates as well as a minor quantity (1–9%) of phosphonates.

All the structures of phosphorus compounds (phosphates and phosphonates) detected by XPS and ³¹P MAS NMR methods have acidic properties and therefore impart the carbon surface an acidic character. The presence of phosphorus-containing compounds gives carbon the ability to absorb metal cations. Polyimide-derived carbon obtained with phosphoric acid has a large sorption capacity for copper, which exceeds adsorption by ion-exchange resins with carboxyl or sulfo groups. Despite having a lower cation-exchange capacity, phosphorus-containing carbon removes more copper than ion-exchange resins. This shows that phosphorus-containing carbon has a higher affinity for copper ions than ion-exchange resins. Phosphorus-containing polyimide-derived carbon is a potential adsorbent for the concentration, separation, or removal of harmful metal contaminants from potable water, wastewater, and other aqueous environments due to its high adsorption capacity for metal cations.

Author Contributions: Investigation, O.I.P., M.S. (Magdalena Sobiesiak) and M.S. (Myroslav Sprynsky); Supervision, A.M.P.; Writing—original draft, A.M.P.; Writing—review & editing, B.G. All authors have read and agreed to the published version of the manuscript.

Funding: This research received no external funding.

Conflicts of Interest: The authors declare no conflict of interest.

References

1. Rodríguez-Reinoso, F. Production and Applications of Activated Carbons. In *Handbook of Porous Solids*; Schüth, F., Sing, K.S.W., Weitkamp, J., Eds.; Wiley: Weinheim, Germany, 2002; Volume 3, pp. 1766–1827. ISBN 9783527618286.
2. Marsh, H.; Rodríguez-Reinoso, F. *Activated Carbon*; Elsevier Ltd.: Oxford, UK, 2006; ISBN 978-0-08-044463-5.
3. Menéndez-Díaz, J.A.; Martín-Gullón, I. Types of Carbon Adsorbents and Their Production. In *Activated Carbon Surfaces in Environmental Remediation*; Bandosz, T.J., Ed.; Interface Science and Technology; Academic Press: Amsterdam, The Netherlands, 2006; Volume 7, pp. 1–47.
4. Kwiatkowski, J.F. (Ed.) *Activated Carbon: Classifications, Properties and Applications*; Nova Science Publishers: New York, NY, USA, 2012; Volume 66, ISBN 9781620816660.
5. Henning, K.-D.; von Kienle, H. Carbon, 5. Activated Carbon. In *Ullmann's Encyclopedia of Industrial Chemistry*; Wiley-VCH Verlag GmbH & Co. KGaA: Weinheim, Germany, 2012; Volume 6, pp. 771–796.

6. Çeçen, F. Activated Carbon. In *Kirk-Othmer Encyclopedia of Chemical Technology*; John Wiley & Sons, Inc.: Hoboken, NJ, USA, 2014; pp. 1–34.
7. Rodríguez-Reinoso, F.; Silvestre-Albero, J. Activated Carbon and Adsorption. In *Reference Module in Materials Science and Materials Engineering*; Elsevier: Amsterdam, The Netherlands, 2016; pp. 1–14. ISBN 9780128035818.
8. Macías-García, A.; Díaz-Díez, M.A.; Gómez-Serrano, V.; González, M.C.F. Preparation and Characterization of Activated Carbons Made up from Different Woods by Chemical Activation with H_3PO_4 . *Smart Mater. Struct.* **2003**, *12*, N24–N28. [[CrossRef](#)]
9. Muñoz, Y.; Arriagada, R.; Soto-Garrido, G.; García, R. Phosphoric and Boric Acid Activation of Pine Sawdust. *J. Chem. Technol. Biotechnol.* **2003**, *78*, 1252–1258. [[CrossRef](#)]
10. Attia, A.A.; Girgis, B.S.; Khedr, S.A. Capacity of Activated Carbon Derived from Pistachio Shells by H_3PO_4 in the Removal of Dyes and Phenolics. *J. Chem. Technol. Biotechnol.* **2003**, *78*, 611–619. [[CrossRef](#)]
11. Diao, Y.; Walawender, W.P.; Fan, L.T. Activated Carbons Prepared from Phosphoric Acid Activation of Grain Sorghum. *Bioresour. Technol.* **2002**, *81*, 45–52. [[CrossRef](#)]
12. Puziy, A.M.; Poddubnaya, O.I.; Gawdzik, B.; Tascón, J.M.D. Phosphorus-Containing Carbons: Preparation, Properties and Utilization. *Carbon* **2020**, *157*, 796–846. [[CrossRef](#)]
13. Benaddi, H.; Legras, D.; Rouzaud, J.-N.; Béguin, F. Influence of the Atmosphere in the Chemical Activation of Wood by Phosphoric Acid. *Carbon* **1998**, *36*, 306–309. [[CrossRef](#)]
14. Xu, T.; Liu, X. Peanut Shell Activated Carbon: Characterization, Surface Modification and Adsorption of Pb^{2+} from Aqueous Solution. *Chin. J. Chem. Eng.* **2008**, *16*, 401–406. [[CrossRef](#)]
15. Puziy, A.M.; Poddubnaya, O.I.; Ziatdinov, A.M. On the Chemical Structure of Phosphorus Compounds in Phosphoric Acid-Activated Carbon. *Appl. Surf. Sci.* **2006**, *252*, 8036–8038. [[CrossRef](#)]
16. Puziy, A.M.; Poddubnaya, O.I.; Socha, R.P.; Gurgul, J.; Wiśniewski, M. XPS and NMR Studies of Phosphoric Acid Activated Carbons. *Carbon* **2008**, *46*, 2113–2123. [[CrossRef](#)]
17. Huang, C.; Sun, T.; Hulicova-Jurcakova, D. Wide Electrochemical Window of Supercapacitors from Coffee Bean-Derived Phosphorus-Rich Carbons. *ChemSusChem* **2013**, *6*, 2330–2339. [[CrossRef](#)]
18. Castro-Muñiz, A.; Suárez-García, F.; Martínez-Alonso, A.; Tascón, J.M.D. Activated Carbon Fibers with a High Content of Surface Functional Groups by Phosphoric Acid Activation of PPTA. *J. Colloid Interface Sci.* **2011**, *361*, 307–315. [[CrossRef](#)] [[PubMed](#)]
19. Carriazo, D.; Gutiérrez, M.C.; Picó, F.; Rojo, J.M.; Fierro, J.L.G.; Ferrer, M.L.; del Monte, F. Phosphate-Functionalized Carbon Monoliths from Deep Eutectic Solvents and Their Use as Monolithic Electrodes in Supercapacitors. *ChemSusChem* **2012**, *5*, 1405–1409. [[CrossRef](#)] [[PubMed](#)]
20. Bairi, V.G.; Bourdo, S.E.; Nasini, U.B.; Ramasahayam, S.K.; Watanabe, F.; Berry, B.C.; Viswanathan, T. Microwave-Assisted Synthesis of Nitrogen and Phosphorus Co-Doped Mesoporous Carbon and Their Potential Application in Alkaline Fuel Cells. *Sci. Adv. Mater.* **2013**, *5*, 1275–1281. [[CrossRef](#)]
21. Xu, J.; Chen, L.; Qu, H.; Jiao, Y.; Xie, J.; Xing, G. Preparation and Characterization of Activated Carbon from Reedy Grass Leaves by Chemical Activation with H_3PO_4 . *Appl. Surf. Sci.* **2014**, *320*, 674–680. [[CrossRef](#)]
22. Fu, R.; Liu, L.; Huang, W.; Sun, P. Studies on the Structure of Activated Carbon Fibers Activated by Phosphoric Acid. *J. Appl. Polym. Sci.* **2003**, *87*, 2253–2261. [[CrossRef](#)]
23. Bedia, J.; Ruiz-Rosas, R.; Rodríguez-Mirasol, J.; Cordero, T. A Kinetic Study of 2-Propanol Dehydration on Carbon Acid Catalysts. *J. Catal.* **2010**, *271*, 33–42. [[CrossRef](#)]
24. Bedia, J.; Barrionuevo, R.; Rodríguez-Mirasol, J.; Cordero, T. Ethanol Dehydration to Ethylene on Acid Carbon Catalysts. *Appl. Catal. B Environ.* **2011**, *103*, 302–310. [[CrossRef](#)]
25. Rosas, J.M.; Ruiz-Rosas, R.; Rodríguez-Mirasol, J.; Cordero, T. Kinetic Study of the Oxidation Resistance of Phosphorus-Containing Activated Carbons. *Carbon* **2012**, *50*, 1523–1537. [[CrossRef](#)]
26. Berenguer, R.; Ruiz-Rosas, R.; Gallardo, A.; Cazorla-Amorós, D.; Morallón, E.; Nishihara, H.; Kyotani, T.; Rodríguez-Mirasol, J.; Cordero, T. Enhanced Electro-Oxidation Resistance of Carbon Electrodes Induced by Phosphorus Surface Groups. *Carbon* **2015**, *95*, 681–689. [[CrossRef](#)]
27. García-Mateos, F.J.; Berenguer, R.; Valero-Romero, M.J.; Rodríguez-Mirasol, J.; Cordero, T. Phosphorus Functionalization for the Rapid Preparation of Highly Nanoporous Submicron-Diameter Carbon Fibers by Electrospinning of Lignin Solutions. *J. Mater. Chem. A* **2018**, *6*, 1219–1233. [[CrossRef](#)]
28. Wang, Y.; Zuo, S.; Yang, J.; Yoon, S.-H. Evolution of Phosphorus-Containing Groups on Activated Carbons during Heat Treatment. *Langmuir* **2017**, *33*, 3112–3122. [[CrossRef](#)]
29. Tebby, J.C. (Ed.) *Handbook of Phosphorus. 31 Nuclear Magnetic Resonance Data (1990)*; CRC Press: Boca Raton, FL, USA, 2017; ISBN 9780203712122.
30. Potrzebowski, M.J.; Kaźmierski, S.; Kassassir, H.; Miksa, B. Phosphorus-31 NMR Spectroscopy of Condensed Matter. In *Annual Reports on NMR Spectroscopy*; Elsevier: Amsterdam, The Netherlands, 2010; Volume 70, pp. 35–114. ISBN 9780123813534.
31. Jagtoyen, M.; Thwaites, M.; Stencil, J.M.; McEnaney, B.; Derbyshire, F. Adsorbent Carbon Synthesis from Coals by Phosphoric Acid Activation. *Carbon* **1992**, *30*, 1089–1096. [[CrossRef](#)]
32. Wiśniewski, M.; Pacholczyk, A.; Terzyk, A.P.; Rychlicki, G. New Phosphorus-Containing Spherical Carbon Adsorbents as Promising Materials in Drug Adsorption and Release. *J. Colloid Interface Sci.* **2011**, *354*, 891–894. [[CrossRef](#)] [[PubMed](#)]

33. Latorre-Sánchez, M.; Primo, A.; García, H. P-Doped Graphene Obtained by Pyrolysis of Modified Alginate as a Photocatalyst for Hydrogen Generation from Water-Methanol Mixtures. *Angew. Chem. Int. Ed.* **2013**, *52*, 11813–11816. [CrossRef]
34. MacIntosh, A.R.; Jiang, G.; Zamani, P.; Song, Z.; Riese, A.; Harris, K.J.; Fu, X.; Chen, Z.; Sun, X.; Goward, G.R. Phosphorus and Nitrogen Centers in Doped Graphene and Carbon Nanotubes Analyzed through Solid-State NMR. *J. Phys. Chem. C* **2018**, *122*, 6593–6601. [CrossRef]
35. Das, T.K.; Banerjee, S.; Sharma, P.; Sudarsan, V.; Sastry, P.U. Nitrogen Doped Porous Carbon Derived from EDTA: Effect of Pores on Hydrogen Storage Properties. *Int. J. Hydrogen Energy* **2018**, *43*, 8385–8394. [CrossRef]
36. Albero, J.; Vidal, A.; Migani, A.; Concepción, P.; Blancafort, L.; García, H. Phosphorus-Doped Graphene as a Metal-Free Material for Thermochemical Water Reforming at Unusually Mild Conditions. *ACS Sustain. Chem. Eng.* **2019**, *7*, 838–846. [CrossRef]
37. Singh, A.S.; Advani, J.H.; Biradar, A.V. Phosphonate Functionalized Carbon Spheres as Brønsted Acid Catalysts for the Valorization of Bio-Renewable α -Pinene Oxide to Trans-Carveol. *Dalton Trans.* **2020**, *49*, 7210–7217. [CrossRef]
38. Matynia, T.; Gawdzik, B.; Chmielewska, E. Synthesis and Properties of Porous Copolymers of 4,4'-Bismaleimido Diphenyl Methane and Styrene. *J. Appl. Polym. Sci.* **1996**, *60*, 1971–1975. [CrossRef]
39. Puziy, A.M.; Poddubnaya, O.I.; Gawdzik, B.; Sobiesiak, M.; Dziadko, D. Heterogeneity of Synthetic Carbons Obtained from Polyimides. *Appl. Surf. Sci.* **2002**, *196*, 89–97. [CrossRef]
40. Puziy, A.M.; Poddubnaya, O.I.; Gawdzik, B.; Sobiesiak, M.; Tsyba, M.M. Functionalization of Carbon and Silica Gel by Phosphoric Acid. *Adsorpt. Sci. Technol.* **2007**, *25*, 531–542. [CrossRef]
41. Puziy, A.M.; Poddubnaya, O.I.; Sobiesiak, M.; Gawdzik, B. Structural and Surface Heterogeneity of Phosphorus-Containing Polyimide-Derived Carbons: Effect of Heat Treatment Temperature. *Adsorption* **2013**, *19*, 717–722. [CrossRef]
42. Sobiesiak, M.; Gawdzik, B.; Puziy, A.M.; Poddubnaya, O.I. Phosphoric Acid and Steam as Activation Agents for Carbonized Porous Polymer Surfaces. *Adsorpt. Sci. Technol.* **2006**, *24*, 167–176. [CrossRef]
43. Sobiesiak, M.; Gawdzik, B.; Puziy, A.M.; Poddubnaya, O.I. Polymer-Based Carbon Adsorbents Obtained from Copolymer of 4,4'-Bis(Maleimidodiphenyl)Methane and Divinylbenzene for Use in SPE. *Chromatographia* **2006**, *64*, 175–181. [CrossRef]
44. Jagiello, J.; Olivier, J.P. A Simple Two-Dimensional NLDFT Model of Gas Adsorption in Finite Carbon Pores. Application to Pore Structure Analysis. *J. Phys. Chem. C* **2009**, *113*, 19382–19385. [CrossRef]
45. Jagiello, J.; Olivier, J.P. 2D-NLDFT Adsorption Models for Carbon Slit-Shaped Pores with Surface Energetical Heterogeneity and Geometrical Corrugation. *Carbon* **2013**, *55*, 70–80. [CrossRef]
46. Jagiello, J.; Olivier, J.P. Carbon Slit Pore Model Incorporating Surface Energetical Heterogeneity and Geometrical Corrugation. *Adsorption* **2013**, *19*, 777–783. [CrossRef]
47. Rouquerol, J.; Llewellyn, P.; Rouquerol, F. Is the BET Equation Applicable to Microporous Adsorbents. In *COPS-7: Characterization of Porous Solids VII*; Llewellyn, P.L., Rodriguez-Reinoso, F., Rouquerol, J., Seaton, N., Eds.; Studies in Surface Science and Catalysis; Elsevier: Amsterdam, The Netherlands, 2007; Volume 160, pp. 49–56.
48. Moulder, J.F.; Stickle, W.F.; Sobol, P.E.; Bomben, K.D. *Handbook of X-ray Photoelectron Spectroscopy*, 2nd ed.; Chastain, J., Ed.; Perkin-Elmer: Eden Prairie, MN, USA, 1992; ISBN 9780962702624.
49. Naumkin, A.V.; Kraut-Vass, A.; Gaarenstroom, S.W.; Powell, C.J. NIST X-ray Photoelectron Spectroscopy Database, NIST Standard Reference Database Number 20, National Institute of Standards and Technology, Gaithersburg MD, 20899. 2000. Available online: <https://doi.org/10.18434/T4T88K> (accessed on 26 August 2022).
50. Scofield, J.H. Hartree-Slater Subshell Photoionization Cross-Sections at 1254 and 1487 EV. *J. Electron Spectros. Relat. Phenom.* **1976**, *8*, 129–137. [CrossRef]
51. Lützenkirchen, J.; Preočanin, T.; Kovačević, D.; Tomišić, V.; Lövgren, L.; Kallay, N. Potentiometric Titrations as a Tool for Surface Charge Determination. *Croat. Chem. Acta* **2012**, *85*, 391–417. [CrossRef]
52. del Piero, S.; Melchior, A.; Polese, P.; Portanova, R.; Tolazzi, M. A Novel Multipurpose Excel Tool for Equilibrium Speciation Based on Newton-Raphson Method and on a Hybrid Genetic Algorithm. *Ann. Chim.* **2006**, *96*, 29–49. [CrossRef]
53. Provencher, S.W. A Constrained Regularization Method for Inverting Data Represented by Linear Algebraic or Integral Equations. *Comput. Phys. Commun.* **1982**, *27*, 213–227. [CrossRef]
54. Provencher, S.W. CONTIN: A General Purpose Constrained Regularization Program for Inverting Noisy Linear Algebraic and Integral Equations. *Comput. Phys. Commun.* **1982**, *27*, 229–242. [CrossRef]
55. Puziy, A.M.; Matynia, T.; Gawdzik, B.; Poddubnaya, O.I. Use of CONTIN for Calculation of Adsorption Energy Distribution. *Langmuir* **1999**, *15*, 6016–6025. [CrossRef]
56. Puziy, A.M.; Poddubnaya, O.I.; Ritter, J.A.; Ebner, A.D.; Holland, C.E. Elucidation of the Ion Binding Mechanism in Heterogeneous Carbon-Composite Adsorbents. *Carbon* **2001**, *39*, 2313–2324. [CrossRef]
57. Thommes, M.; Kaneko, K.; Neimark, A.V.; Olivier, J.P.; Rodríguez-Reinoso, F.; Rouquerol, J.; Sing, K.S.W. Physisorption of Gases, with Special Reference to the Evaluation of Surface Area and Pore Size Distribution (IUPAC Technical Report). *Pure Appl. Chem.* **2015**, *87*, 1051–1069. [CrossRef]
58. Myglovets, M.; Poddubnaya, O.I.; Sevastyanova, O.; Lindström, M.E.; Gawdzik, B.; Sobiesiak, M.; Tsyba, M.M.; Sapsay, V.I.; Klymchuk, D.O.; Puziy, A.M. Preparation of Carbon Adsorbents from Lignosulfonate by Phosphoric Acid Activation for the Adsorption of Metal Ions. *Carbon* **2014**, *80*, 771–783. [CrossRef]

59. Puziy, A.M.; Poddubnaya, O.I.; Sobiesiak, M.; Gawdzik, B. Assessment of the Structural Evolution of Polyimide-Derived Carbons Obtained by Phosphoric Acid Activation Using Fourier Transform Infrared and Raman Spectroscopy. *Adsorpt. Sci. Technol.* **2017**, *35*, 403–412. [[CrossRef](#)]
60. Jackson, S.T.; Nuzzo, R.G. Determining Hybridization Differences for Amorphous Carbon from the XPS C 1s Envelope. *Appl. Surf. Sci.* **1995**, *90*, 195–203. [[CrossRef](#)]
61. Haerle, R.; Riedo, E.; Pasquarello, A.; Baldereschi, A. Sp^2/Sp^3 Hybridization Ratio in Amorphous Carbon from C 1s Core-Level Shifts: X-ray Photoelectron Spectroscopy and First-Principles Calculation. *Phys. Rev. B* **2001**, *65*, 32–37. [[CrossRef](#)]
62. Pandiyani, R.; Deegan, N.; Dirany, A.; Drogui, P.; El Khakani, M.A. Correlation of Sp^2 Carbon Bonds Content in Magnetron-Sputtered Amorphous Carbon Films to Their Electrochemical H_2O_2 Production for Water Decontamination Applications. *Carbon* **2015**, *94*, 988–995. [[CrossRef](#)]
63. Mominuzzaman, S.M.; Alam, M.; Soga, T.; Jimbo, T. Rearrangements of Sp^2/Sp^3 Hybridized Bonding with Phosphorus Incorporation in Pulsed Laser Deposited Semiconducting Carbon Films by X-ray Photoelectron Spectroscopic Analysis. *Diam. Relat. Mater.* **2006**, *15*, 1795–1798. [[CrossRef](#)]
64. Kelemen, S.R.; Rose, K.D.; Kwiatek, P.J. Carbon Aromaticity Based on XPS Π to Π^* Signal Intensity. *Appl. Surf. Sci.* **1993**, *64*, 167–174. [[CrossRef](#)]
65. Gardella, J.A.; Ferguson, S.A.; Chin, R.L. $\Pi^* \leftarrow \pi$ Shakeup Satellites for the Analysis of Structure and Bonding in Aromatic Polymers by X-ray Photoelectron Spectroscopy. *Appl. Spectrosc.* **1986**, *40*, 224–232. [[CrossRef](#)]
66. Sydorchuk, V.; Poddubnaya, O.I.; Tsyba, M.M.; Zakutevskyy, O.; Khyzhun, O.; Khalameida, S.; Puziy, A.M. Photocatalytic Degradation of Dyes Using Phosphorus-Containing Activated Carbons. *Appl. Surf. Sci.* **2021**, *535*, 147667. [[CrossRef](#)]
67. Delobel, R.; Le Bras, M.; Ouassou, N.; Descressain, R. Fire Retardance of Polypropylene by Diammonium Pyrophosphate-Pentaerythritol: Spectroscopic Characterization of the Protective Coatings. *Polym. Degrad. Stab.* **1990**, *30*, 41–56. [[CrossRef](#)]
68. Bourbigot, S.; Le Bras, M.; Delobel, R. Carbonization Mechanisms Resulting from Intumescence Association with the Ammonium Polyphosphate-Pentaerythritol Fire Retardant System. *Carbon* **1993**, *31*, 1219–1230. [[CrossRef](#)]
69. Bourbigot, S.; Le Bras, M.; Delobel, R.; Trémillon, J.-M. Synergistic Effect of Zeolite in an Intumescence Process. Study of the Interactions between the Polymer and the Additives. *J. Chem. Soc. Faraday Trans.* **1996**, *92*, 3435–3444. [[CrossRef](#)]
70. Bourbigot, S.; Le Bras, M.; Delobel, R.; Decressain, R.; Amoureux, J.-P. Synergistic Effect of Zeolite in an Intumescence Process: Study of the Carbonaceous Structures Using Solid-State NMR. *J. Chem. Soc. Faraday Trans.* **1996**, *92*, 149–158. [[CrossRef](#)]
71. Krawietz, T.R.; Lin, P.; Lotterhos, K.E.; Torres, P.D.; Barich, D.H.; Clearfield, A.; Haw, J.F. Solid Phosphoric Acid Catalyst: A Multinuclear NMR and Theoretical Study. *J. Am. Chem. Soc.* **1998**, *120*, 8502–8511. [[CrossRef](#)]
72. Glonek, T.; Van Wazer, J.R. Phosphorus-31 Spin-Lattice Relaxation of Esters of Orthophosphoric Acid. *J. Phys. Chem.* **1976**, *80*, 639–643. [[CrossRef](#)]
73. Hayashi, S.; Hayamizu, K. High-Resolution Solid-State ^{31}P NMR of Alkali Phosphates. *Bull. Chem. Soc. Jpn.* **1989**, *62*, 3061–3068. [[CrossRef](#)]
74. Jagtoyen, M.; Derbyshire, F. Activated Carbons from Yellow Poplar and White Oak by H_3PO_4 Activation. *Carbon* **1998**, *36*, 1085–1097. [[CrossRef](#)]
75. Harris, R.K.; Merwin, L.H.; Hägele, G. Corrigendum to Solid-State Nuclear Magnetic Resonance Study of a Series of Phosphonic and Phosphinic Acids. *J. Chem. Soc. Faraday Trans. 1* **1989**, *85*, 3899–3900. [[CrossRef](#)]
76. Westall, J. Chemical Equilibrium Including Adsorption on Charged Surfaces. In *Particulates in Water*; Kavanaugh, M.C., Leckie, J.O., Eds.; Advances in Chemistry Series; American Chemical Society: Washington, DC, USA, 1980; Volume 189, pp. 33–44. ISBN 0-8412-0499-3.
77. Puziy, A.M.; Poddubnaya, O.I.; Zaitsev, V.N.; Konoplińska, O.P. Modeling of Heavy Metal Ion Binding by Phosphoric Acid Activated Carbon. *Appl. Surf. Sci.* **2004**, *221*, 421–429. [[CrossRef](#)]
78. Lützenkirchen, J. (Ed.) *Surface Complexation Modelling*; Interface Science and Technology; Elsevier: Amsterdam, The Netherlands, 2006; Volume 11, ISBN 978-0-12-372572-1.
79. Goldberg, S. Surface Complexation Modeling. In *Reference Module in Earth Systems and Environmental Sciences*; Elsevier: Amsterdam, The Netherlands, 2013; pp. 1–14. ISBN 9780124095489.
80. Zhang, Y.; Luo, W. Adsorptive Removal of Heavy Metal from Acidic Wastewater with Biochar Produced from Anaerobically Digested Residues: Kinetics and Surface Complexation Modeling. *BioResources* **2014**, *9*, 2484–2499. [[CrossRef](#)]
81. Sánchez-Polo, M.; Rivera-Utrilla, J. Adsorbent–adsorbate Interactions in the Adsorption of Cd(II) and Hg(II) on Ozonized Activated Carbons. *Environ. Sci. Technol.* **2002**, *36*, 3850–3854. [[CrossRef](#)]
82. Rivera-Utrilla, J.; Sánchez-Polo, M. Adsorption of Cr(III) on Ozonised Activated Carbon. Importance of $C\pi$ —Cation Interactions. *Water Res.* **2003**, *37*, 3335–3340. [[CrossRef](#)]
83. Leon y Leon, C.A.; Solar, J.M.; Calemma, V.; Radovic, L.R. Evidence for the Protonation of Basal Plane Sites on Carbon. *Carbon* **1992**, *30*, 797–811. [[CrossRef](#)]
84. Álvarez-Merino, M.A.; López-Ramón, M.V.; Moreno-Castilla, C. A Study of the Static and Dynamic Adsorption of Zn(II) Ions on Carbon Materials from Aqueous Solutions. *J. Colloid Interface Sci.* **2005**, *288*, 335–341. [[CrossRef](#)]
85. Montes-Morán, M.A.; Menéndez, J.A.; Fuente, E.; Suárez, D. Contribution of the Basal Planes to Carbon Basicity: An Ab Initio Study of the $H_3O^+ - \pi$ Interaction in Cluster Models. *J. Phys. Chem. B* **1998**, *102*, 5595–5601. [[CrossRef](#)]